Latin American Journal of Solids and Structures
www.lajss.org

# Interaction Analysis of Non-aligned Cracks Using Extended Finite Element Method

**Abstract**

Multiple flaws are frequently occurred in actual components, such as pressure vessels and power plants. These flaws will in some circumstances lead to more severe effects than single flaw alone. Assessment of the interaction behavior is based on the evaluation of alignment and combination of these multiple flaws. In the current standards, multiple cracks are treated as an equivalent single crack if the distance between two cracks satisfies a prescribed criterion. First, this study introduces the current alignment and combination rules for through-wall cracks. Following, to investigate the effects of the interaction of cracks, brittle fracture of a plate containing two offset cracks is simulated. The effect of cracks distances and crack lengths on stress intensity factors is evaluated. In addition, crack growth behavior is simulated based on linear elastic fracture mechanics approach. The extended finite element method has been utilized to model the problem. This method enables the domain to be modeled by finite elements without explicitly meshing the crack surfaces, and hence crack propagation simulations can be carried out without remeshing. Based on the results, a new alignment and combination rule is proposed.

**Keywords**

crack interaction, crack growth, extended finite element method, brittle fracture.

**Ali Abbaszadeh Bidokhti** [a]
**Amir Reza Shahani** [b]

[a] PhD Candidate, Faculty of Mechanical Engineering, K.N. Toosi University of Technology, Tehran, Iran
E-mail: abbaszadeh@dena.kntu.ac.ir
[b] Prof., Faculty of Mechanical Engineering, K. N. Toosi University of Technology, Tehran, Iran

http://dx.doi.org/10.1590/1679-78251664

Received 25.10.2014
In Revised Form 10.06.2015
Accepted 20.07.2015
Available online 03.08.2015

## 1 INTRODUCTION

Engineering structures may contain flaws during the fabrication process or plant operation. The structural significance of such flaws particularly cracks needs to be assessed to prevent failure of the component during the service life. If a crack is detected in a component, an assessment is required in accordance with a respective code or analysis whether that part can continue to function or it should be replaced. Multiple cracks are often encountered in actual components, such as power plants, and the advanced nuclear reactors. The interaction of multiple cracks has received significant attention in recent years, mainly because it presents a very important issue in the prediction of component life (Jones, Atluri, Pitt, & Williams, 1995; Lam & Phua, 1991; Tan & Chen, 2013). When such crack colonies are present in a component or structure, the failure event is usually preceded by the interaction and coalescence of those cracks. The coalescence of multiple cracks causes an abrupt increase in crack size and accelerates the crack growth. Non-aligned multiple cracks are occasionally called *offset* or *parallel* cracks. Multiple interacting offset cracks are combined and treated as an equivalent single larger crack if the distance between two cracks satisfies a prescribed criterion so that the existing methods for fracture analysis can be applied. In an engineering assessment for fitness-for-service (FFS), the influence of interaction on crack growth is taken into account conservatively by applying alignment and combination rules. The first process to be assessed in the case cracks occur in different cross-sections is alignment. For critical values of the spacing distance between the cracks, alignment needs to be done in the same cross-section; In other words, when multiple cracks comply with the alignment rule, aligned cracks should be treated as coplanar cracks. Following, if multiple coplanar cracks exist, each crack should be checked for interaction with each of the neighbors using the original crack dimensions. If the distance between two cracks satisfies the combination rule, they are combined as an equivalent single crack. In the current fitness-for-service codes, such as ASME Code Section XI (ASME, 2010), JSME Code (JSME, 2004), BS 7910 (BS, 2005), API 579(API, 2007), WES 2805 (WES, 1997), GB/T 19624 (CS, 2004), European FITNET Project (European Fitness for Service Network, 2008), RCC-MR A16 (Commissariat a L' Energie Atomique, 2002), FKM (FKM, 2004), RSE-M Code (AFCEN, 2005), R6 (British Energy Generation Ltd., 2006), the alignment and combination rules have been proposed. For two typical styles of through-wall offset cracks, as shown in Fig.1, the treatment rules of multiple cracks in fitness-for-service codes are listed in Table 1. As can be seen in Table 1, alignment and combination rules in the FFS codes are different from each other. Therefore, it is expected to obtain different results for the remaining life, and safety margin for a cracked component. The question is whether these rules are either unsafe or unnecessarily conservative. For example, an absolute value 12.5 mm (as shown in Table 1) is used as an alignment rule in ASME Code Section XI. This indicates that the interaction is not taken into account even if it is important for large cracks. Most of the alignment and combination rules in Table 1 are designed to enable safe rather than particularly realistic assessment.

| Standard/codes | Alignment rules | Combination rules |
|---|---|---|
| ASME | $H \leq 12.5$ mm | $S \leq \max(2a_1, 2a_2)$ |
| JSME | Growth : $H \leq 10$ mm $if$ $S \leq 5$ mm<br>$H \leq 2S$ $if$ $S > 5$ $mm$<br>Fracture: $H \leq 12.5$ mm | $S \leq \max(2a_1, 2a_2)$ |
| API 579 | $S < 0$: $H \leq (a_1 + a_2)$<br>$S > 0$: $H \leq (a_1 + a_2)$& $S \leq (a_1 + a_2)$ | $S \leq a_1 + a_2$ |
| BS 7910 | $D \leq (a_1 + a_2)$ | $S \leq \min(2a_1, 2a_2)$ |
| WES 2805 | $H \leq 0.5 \min(2a_1, 2a_2)$ | $S \leq \max(2a_1, 2a_2)$ |
| GB/T 19624 | $H \leq \min(2a_1, 2a_2)$ | $S \leq \min(2a_1, 2a_2)$ |
| R6 | $D \leq (a_1 + a_2)$ | $S \leq \min(2a_1, 2a_2)$ |
| A16 | $D \leq (a_1 + a_2)$ | $S \leq \min(2a_1, 2a_2)$ |
| FKM | $D \leq (a_1 + a_2)$ | $S \leq \min(2a_1, 2a_2)$ |
| RSE-M | Interaction rectangles | Interaction rectangles |
| FITNET | $H \leq \min(2a_1, 2a_2)$ | $S \leq \min(2a_1, 2a_2)$ |

**Table 1:** cracks treatment rules for through-wall cracks in the fitness-for-service codes.

Extensive studies have been conducted to understand the effect of multiple crack interaction and to reduce the conservativeness in the current assessment procedures. In addition, many approaches have been developed to provide insights on the interacting effect of multiple cracks under linear elastic fracture mechanics (LEFM). Some analytical models have been proposed for the problem of a linear elastic solid with multiple cracks. Yokobori et al. (Yokobori, Uozumi, & Ichikawa, 1971) based on the concept of continuous distribution of infinitesimal dislocations, studied two equal length offset cracks in an infinite elastic solid. Sadowski et al. (Sadowski, Marsavina, Peride, & Craciun, 2009) formulated a new analytical model in order to investigate the interaction of two collinear cracks in an orthotropic elastic material. The solutions are restricted to special geometries.

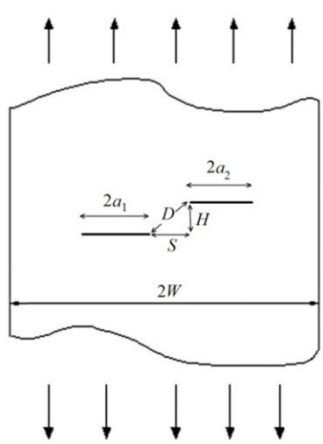


**Figure 1:** Sketch map of offset cracks.

Other approaches such as finite element method (Serier, Belhouari, & Bachir Bouiadjra, 2004), finite element alternating method (Kamaya, 2008) and body force method (Murakami & Nemat-Nasser, 1982) have been developed to provide insights on the interacting effect of multiple cracks. However, these works focused on the calculation of stress intensity factors. The condition of crack coalescence for offset cracks is often studied experimentally due to the difficulty of simulation of the crack growth process. Hasegawa et al. (Hasegawa, Saito, & Miyazaki, 2009) performed fracture experiments on carbon steel plates with two nonaligned flaws and proposed a new alignment rule for linear elastic fracture mechanics evaluation. Miyazaki et al. (Miyazaki, Hasegawa, Saito, & Bezensek, 2009) conducted fracture tests on flat plate specimen with non-aligned flaws at ambient temperature and investigated the effects of the flaw separation and flaw size on the maximum load. Although many attempts have been done to study the interaction of multiple cracks, but it is an open problem. Some FFS codes have been revisited in recent years. The reason for revision of FFS codes is to reduce the margin of conservativeness of these codes to extend the component life and reduce the costs of the component replacement. This reason justifies the new studies of interacting cracks and revision of FFS codes. This has been done based on new simulations, new softwares, new tools, and new methods that were not available before. Certainly, extended finite element method (X-FEM) is an appropriate tool for handling huge computations and crack growth simulations.

In the present study a new application of X-FEM is developed for simulating the growth of multiple interacting cracks in a brittle material. The model developed based on the principles of mixed mode fracture mechanics, provides a rational explanation for the phenomenon of crack interaction, and predicts the coalescence conditions. The X-FEM allows the entire crack to be represented independently of the finite element mesh, and so remeshing is not necessary to model crack growth. So, in this study, the interaction between two non-aligned parallel through-wall cracks is investigated considering their length, distance between planes and crack tip separation. The values of mode-I and mode-II stress intensity factors are evaluated by X-FEM analysis and the effect of stress intensity factor interaction on fracture behavior is studied. In addition, the crack growth simulation is developed using the X-FEM and propagation paths of two interacting cracks have been determined. The interaction is considered by the occurrence of coalescence. Based on the simulation results, new alignment and combination rules are proposed for linear elastic fracture mechanics

## 2 EXTENDED FINITE ELEMENT METHOD

The extended finite element method (X-FEM) proposed by Moës et al. (Moës, Dolbow, & Belytschko, 1999) proved to be a very efficient tool for the numerical modeling of crack propagation in LEFM. In the X-FEM, a discontinuous function and the two-dimensional asymptotic crack-tip displacement fields are added to the finite element approximation to account for the crack using the notion of partition of unity. This allows the representation of crack discontinuities independently of the mesh. The method does not require any remeshing for crack growth. The extended finite element approximation for the displacement is expressed as:

$$\mathbf{u}^h(\mathbf{x}) = \sum_{i\in I} N_i(\mathbf{x})\boldsymbol{u}_i + \sum_{j\in J} N_j(\mathbf{x})H(\mathbf{x})\mathbf{a}_j + \sum_{k\in K} N_k(\mathbf{x})\left(\sum_{l=1}^{4} \Psi_l(\mathbf{x})\mathbf{b}_k^l\right) \tag{1}$$

where $I$ is the set of all nodes in the mesh; $\mathbf{u}_i$ is the classical degree of freedom at node $i$; $N_i$ is the shape function associated with node $i$; $J \subset I$ is the subset of nodes that are enriched for the crack discontinuity and $\mathbf{a}_i$ are the corresponding additional degrees of freedom; the nodes in $J$ are such that their support intersects the crack but do not contain any of its crack tips; and $K \subset I$ is the subset of nodes that are enriched for the crack tip. The corresponding additional degrees of freedom are $\mathbf{b}_k^l$, l=1, ..., 4, for the crack tip; the nodes in $K$ are such that their support contain the crack tip. The function $H(\mathbf{x})$ is a discontinuous function across the crack surface and is constant on each side of the crack: $+1$ on one side of the crack and $-1$ on the other. The near-tip functions $\Psi_l(\mathbf{x})$; $l$=1, ..., 4 are given by

$$\{\Psi_l(r,\theta)\}, \qquad l = 1 \dots 4 = \left[\sqrt{r}sin\frac{\theta}{2}, \sqrt{r}cos\frac{\theta}{2}, \sqrt{r}sin\frac{\theta}{2}sin\theta, \sqrt{r}cos\frac{\theta}{2}sin\theta\right] \tag{2}$$

where $(r,\ \theta)$ are the local polar co-ordinates at the crack tip. The variational formulation of the boundary value problem is given by

$$\int_{\Omega} \boldsymbol{\sigma} : \delta\boldsymbol{\varepsilon}\, d\Omega = \int_{\Omega} \boldsymbol{b}.\, \delta\boldsymbol{\varepsilon}\, d\Omega + \int_{\Gamma_t} \bar{\boldsymbol{t}}.\, \delta\boldsymbol{\varepsilon}\, d\Gamma \tag{3}$$

where $\boldsymbol{\sigma}$ is the stress tensor, $\boldsymbol{\varepsilon}$ is the strain tensor, and $\boldsymbol{b}$ and $\bar{\boldsymbol{t}}$ are the body force and external traction vectors, respectively. $\Omega$ is the domain and $\Gamma_t$ is traction boundary. Discretization of Eq.3 and applying X-FEM displacement approximation (Eq. 1) results in a discrete system of linear equilibrium equations:

$$\mathbf{K}\mathbf{u}^h = \mathbf{f} \tag{4}$$

where $\mathbf{K}$ is the stiffness matrix, $\mathbf{u}^h$ is the vector of degrees of nodal freedom (for both classical and enriched ones) and $\mathbf{f}$ is the vector of external force. The element contribution to K and f are as follows:

$$\mathbf{K}_{ij}^e = \begin{bmatrix} \mathbf{K}_{ij}^{\mathrm{uu}} & \mathbf{K}_{ij}^{\mathrm{ua}} & \mathbf{K}_{ij}^{\mathrm{ub}} \\ \mathbf{K}_{ij}^{\mathrm{au}} & \mathbf{K}_{ij}^{\mathrm{aa}} & \mathbf{K}_{ij}^{\mathrm{ab}} \\ \mathbf{K}_{ij}^{\mathrm{bu}} & \mathbf{K}_{ij}^{\mathrm{bu}} & \mathbf{K}_{ij}^{\mathrm{bb}} \end{bmatrix} \tag{5}$$

$$\mathbf{f}_i^{\mathrm{e}} = \left\{\mathbf{f}_i^{\mathrm{u}} \quad \mathbf{f}_i^{\mathrm{a}} \quad \mathbf{f}_i^{\mathrm{b1}} \quad \mathbf{f}_i^{\mathrm{b2}} \quad \mathbf{f}_i^{\mathrm{b3}} \quad \mathbf{f}_i^{\mathrm{b4}}\right\}^T \tag{6}$$

where the submatrices and vectors that appear in Eq. (5) and Eq. (6) are defined as:

$$\mathbf{K}_{ij}^{rs} = \int_{\Omega^{\mathrm{e}}} (\mathbf{B}_i^r)^{\mathrm{T}}\, \mathbf{D}\, \mathbf{B}_j^s\, d\Omega \qquad (r,s = \mathrm{u},\mathrm{a},\mathrm{b}) \tag{7}$$

$$\mathbf{f}_i^{\mathrm{u}} = \int_{\Gamma_t} N_i \bar{\mathbf{t}}\, d\Gamma + \int_{\Omega^e} N_i \mathbf{b}\, d\Omega \tag{8}$$

$$\mathbf{f}_i^{\mathrm{a}} = \int_{\Gamma_t} N_i H \bar{\mathbf{t}}\, d\Gamma + \int_{\Omega^e} N_i H \mathbf{b}\, d\Omega \tag{9}$$

$$\mathbf{f}_i^{\mathrm{b}\alpha} = \int_{\Gamma_t} N_i F_\alpha \bar{\mathbf{t}}\, d\Gamma + \int_{\Omega^e} N_i F_\alpha \mathbf{b}\, d\Omega \tag{10}$$

In Eq. 7, $\mathbf{D}$ is the constitutive matrix for an isotropic linear elastic material, and $\mathbf{B}_{\mathrm{i}}^{\mathrm{u}}$, $\mathbf{B}_{\mathrm{i}}^{\mathrm{a}}$, and $\mathbf{B}_{\mathrm{i}}^{\mathrm{b}}$ are the matrix of shape function derivatives which are given by

$$\mathbf{B}_i^{\mathrm{u}} = \begin{bmatrix} \boldsymbol{N_{i,x}} & \mathbf{0} \\ \mathbf{0} & \boldsymbol{N_{i,y}} \\ \boldsymbol{N_{i,y}} & \boldsymbol{N_{i,x}} \end{bmatrix} \tag{11}$$

$$\mathbf{B}_i^{\mathrm{a}} = \begin{bmatrix} (\boldsymbol{N_i H})_{,x} & \mathbf{0} \\ \mathbf{0} & (\boldsymbol{N_i H})_{,y} \\ (\boldsymbol{N_i H})_{,y} & (\boldsymbol{N_i H})_{,x} \end{bmatrix} \tag{12}$$

$$\mathbf{B}_i^{\mathrm{b}} = \begin{bmatrix} \mathbf{B}_i^{\mathrm{b1}} & \mathbf{B}_i^{\mathrm{b2}} & \mathbf{B}_i^{\mathrm{b3}} & \mathbf{B}_i^{\mathrm{b4}} \end{bmatrix} \tag{13}$$

$$\mathbf{B}_i^{\mathrm{b}\alpha} = \begin{bmatrix} (\boldsymbol{N_i F_\alpha})_{,x} & \mathbf{0} \\ \mathbf{0} & (\boldsymbol{N_i F_\alpha})_{,y} \\ (\boldsymbol{N_i F_\alpha})_{,y} & (\boldsymbol{N_i F_\alpha})_{,x} \end{bmatrix} \qquad (\alpha = 1,2,3,4) \tag{14}$$

For the elements cut by a crack, the standard Gauss quadrature points are insufficient for numerical integration. The elements that are cut by a crack are subdivided into sub-triangles which do not cross the crack and the element quadrature is performed over these sub-triangles. Therefore, the number of gauss integration points is increased for the elements that have been enriched.

## 3 COMPUTATION OF STRESS INTENSITY FACTORS AND CRACK GROWTH ANALYSIS

Fracture parameters such as the mode-I and mode-II stress intensity factors (SIFs) are determined using the domain form of the interaction integral (Yau, Wang, & Corten, 1980). In the interaction integral method, the 2-d plane strain auxiliary fields are introduced and superposed on the actual fields that arise from the solution of the boundary value problem. By judicious choice of the auxiliary fields, the interaction integral can be directly related to the mixed-mode stress intensity factors. When the interaction integral is recast as an equivalent domain integral, it has the following form:

$$I^{(1,2)} = \int_A \left[\sigma_{ij}^{(1)} \frac{\partial u_i^2}{\partial x_1} + \sigma_{ij}^{(2)} \frac{\partial u_i^1}{\partial x_1} - W^{(1,2)} \delta_{1j}\right] \frac{\partial q}{\partial x_j} dA \tag{15}$$

where $^{(1)}$ are the actual fields of the problem approximated by the X-FEM solution and $^{(2)}$ are the auxiliary fields. These fields are chosen to be the asymptotic crack tip fields for pure mode-I or pure mode-II to compute $K_I$ and $K_{II}$, respectively. In Eq.(15), $x_1$; $x_2$ are the local directions with respect to the crack tip, $\delta_{1j}$ is the Kronecker's delta and $q$ is an arbitrary and continuous function that must vanish at the outer boundary of the problem domain and take the value 1 at the crack tip. The SIFs of the problem are then calculated as follows:

$$K_I = \frac{2}{E'} I^{(1,Pure\ Mode\ I)} \qquad\qquad K_{II} = \frac{2}{E'} I^{(1,Pure\ Mode\ II)} \tag{16}$$

where $E'=E$ for plane stress and $E'=E\ /\ (1-\nu^2)$ for plane strain.

The $q$-function used in this work is an annular weighting function which takes value $q=1$ for nodes contained in a circle of radius $r_q$ measured from the crack tip, and $q=0$ for the remaining nodes. For additional details on the evaluation of the SIFs in the X-FEM, see (Moës et al., 1999).

For the prediction of the crack growth direction, the MTS criterion (maximum tangential stress) (Erdogan & Sih, 1963) is used, which means that the crack will propagate from its tip in a direction $\theta_c$ so that the circumferential stress $\sigma_{\theta\theta}$ is maximum.

$$\theta_c = 2\, arctan\left[\frac{-2K_{II}/K_I}{1+\sqrt{1+8(K_{II}/K_I)^2}}\right] \tag{17}$$

where $\theta_c$ is the angle that will follow the crack for each of the crack increments. $\theta_c$ is measured with respect to a local polar coordinate system with its origin at the crack-tip and aligned with the direction of the existing crack. The sign convention is such that $\theta_c < 0$ when $KII > 0$ and vice-versa. The equivalent mode-I stress intensity factor is calculated using the growth angle $\theta_c$

$$K_I^{eq} = K_I cos^3\left(\frac{\theta_c}{2}\right) - K_{II}\frac{3}{2} cos^3\left(\frac{\theta_c}{2}\right) \sin(\theta_c) \tag{18}$$

This can then be compared to the critical value for the material and crack growth is said to occur if

$$K_I^{eq} \geq K_c \tag{19}$$

where $K_c$ is the critical stress intensity factor, or fracture toughness of the material.

## 4 NUMERICAL SIMULATION

In this section, the X-FEM simulation of two offset cracks on the flat plate is investigated for different parametric studies. Two types of simulations are carried out: In the first, the specimen is subjected to the fixed tensile stress, and stress intensity factors are extracted for different parameters. The specimen in the second type is subjected to displacement control loading, and the growth path of two cracks and their coalescence are analyzed for different conditions.

### 4.1. Model Description

The tensile specimen shown in Fig. 2 is employed for X-FE analysis. The model is a representation of a plate with two non-aligned through-wall cracks. Tensile static load is applied to this plate and brittle fracture was assumed. The mechanical properties of specimen are shown in Table 2.

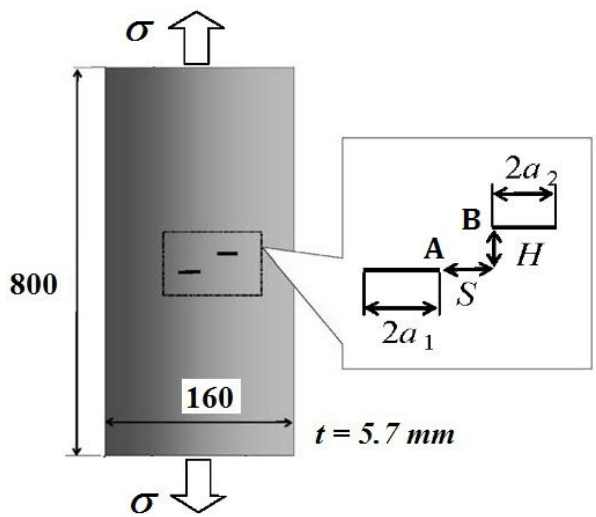


**Figure 2:** Illustration of plate geometry with two nonaligned through-wall cracks.

| Mechanical property | value |
|---|---|
| Young's modulus, $E$ (GPa) | 200 |
| Yield strength, $\sigma_Y$ (MPa) | 304 |
| Tensile strength, $\sigma_U$ (MPa) | 449 |
| Poisson's ration, $\nu$ | 0.3 |
| Fracture toughness, $K_{IC}$ (MPa$\sqrt{\text{m}}$) | 28.2 |
| Elongation % (min.) | 18 |

**Table 2:** Mechanical characteristics of the plate.

The width $W$ and wall-thickness $t$ of the specimen are 160 mm and 5.7 mm, respectively. The length of the specimen is 800 mm. The plate is loaded by a uniform stress in the vertical direction. The plane strain condition is assumed, and a two-dimensional X-FE model has been defined, as depicted in Fig. 3.

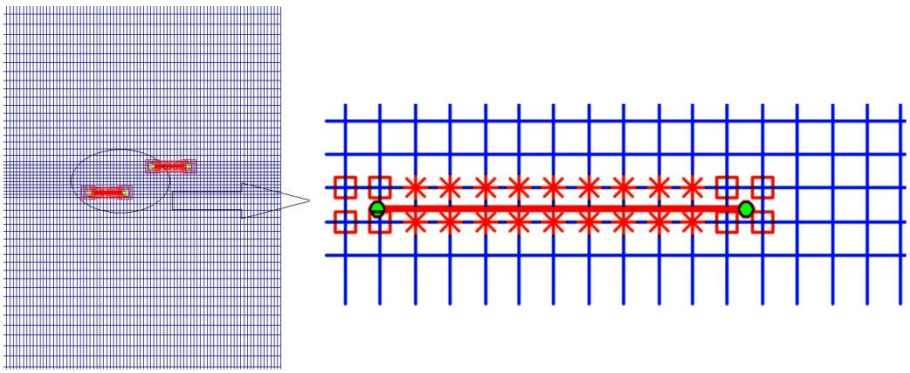

**Figure 3:** Numerical model and mesh detail around two offset cracks with enriched nodes.

The structured mesh consists of 9435 quadrilateral elements. This level of discretization is found to yield a converged solution (results are within 1% of those for a 10000 elements). The mesh is refined to the centre of the plate to obtain more accuracy in the domain of crack propagation. It is independent of the crack geometry and the same mesh is used throughout the simulation. The great advantage of extended finite element method is using a fixed mesh in all performed simulations. Because of a high number of performed analyses, this method is very convenient particularly in the crack growth analysis and tremendously reduces the time of the analysis.

When cracks are dissimilar in length, the larger crack ($2a_1$) is susceptible to fracture. The larger crack is assumed to have constant length, $2a_1$=20 mm. In the analysis, the effects of different values of the out-of-plane crack separation ($H$), the in-plane crack separation ($S$), the direct distance between two cracks ($D$), and the length of smaller crack ($2a_2$) on the stress intensity factors and crack growth path is evaluated. Based on the physics of the problem and according to FFS rules presented in Table 1, new dimensionless variables are defined for parametric analysis of the problem, and the effects of these variables on the variation of stress intensity factor of the cracks and crack coalescence are analyzed:

$$H^* = \frac{H}{2a_2} \qquad S^* = \frac{S}{2a_2} \tag{20}$$

In order to obtain more detailed interactions, the mode-I stress intensity factor at inner tip of larger crack (Fig. 2: point A) is extracted. The $K_{IA}$ is normalized by the stress intensity factor $K_0$ and is referred to $K_{IA}^{*}=K_I/K_0$. Note that $K_0$ is the stress intensity factor for an isolated crack with the length of $2a_1$ under normal remote stress. In this problem the length of first crack is assumed to be fixed, equal to $2a_1$=20 mm, the length of second one ($2a_2$) is selected as a variable and the analyses are carried out for $2a_2$= 20, 10, 5 mm.

### 4.2. Model Verification

To verify the X-FEM model, both two and three-dimensional standard finite element analyses were carried out using the code Abaqus. Quarter-point collapsed elements were introduced at the crack tip to model the stress field singularity. For the 2-D FE model the element type CPS8 (8-node quadratic plane stress) and for the 3-D FE model the type C3D20 (20-node quadratic brick) is used. For comparison of results, a special specimen ($2a_1=2a_2=20$ mm, $H=S=10$ mm i.e. $H^*=S^*=0.5$) is subjected to a prescribed tensile load on its top edge equal to 10000 N/m, and its bottom edge is fixed. The material is identical to the one considered in Table 2. The 2-D FE mesh consists of 3371 elements and 10294 nodes. The 3-D FE mesh consists of 11392 elements and 55153 nodes. The 2-D and 3-D FE meshes used in Abaqus conform to the crack surface. In order to capture singularity at the crack tip, the mesh around the crack tip is needed to be considerably refined. The FE meshes and deformed shapes of the specimen are shown in Fig. 4 and Fig. 5. Also, Fig. 6 shows the normalized mode-I stress intensity factor distribution along thickness for 3-D FE model in Abaqus. It seems that this parameter is approximately fixed along thickness direction. Table 3 compares the results of FE models and X-FE model. The results of X-FE model are consistent with the 2-D and 3-D FE models. It seems that this model could be used for further simulations.

| Model. | Order of elements | No. of elements | No. of nodes | No. of DOFs | Max. displacement | Normalized stress intensity factor $K_{IA}$* |
|---|---|---|---|---|---|---|
| 2-D X-FE | linear | 9435 | 9710 | 19420 | $4.033\times10^{-8}$ | 1.134 |
| 2-D FE | quadratic | 4371 | 11294 | 22588 | $4.034\times10^{-8}$ | 1.138 |
| 3-D FE | quadratic | 11392 | 55153 | 165459 | $4.033\times10^{-8}$ | 1.136 |

**Table 3:** Comparison of the results of different models.

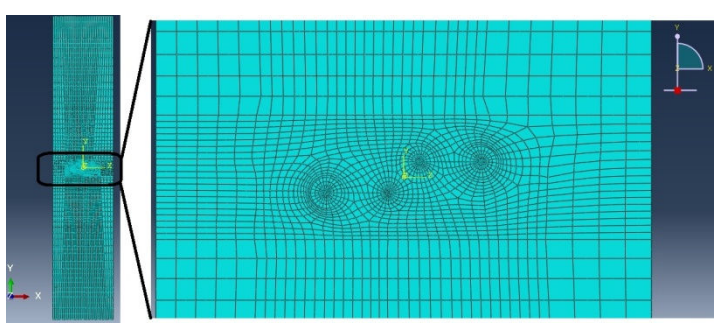

(a)

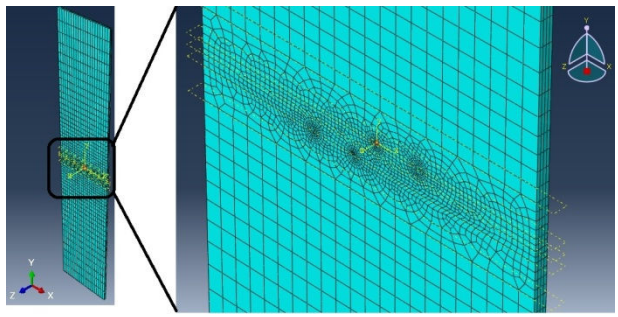

(b)

**Figure 4:** FE models created in Abaqus (a) 2-D mesh (b) 3-D mesh.

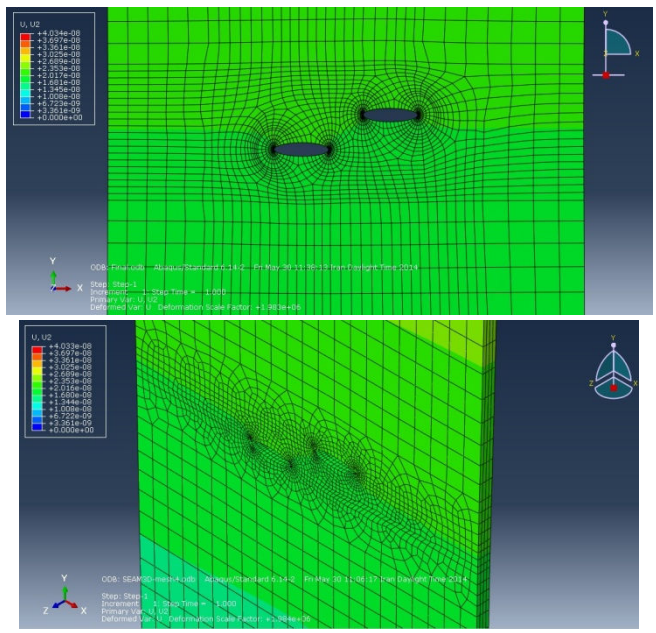

(a)

(b)

**Figure 5:** Deformed shape of the FE models in Abaqus
(a) 2-D FE model (b) 3-D FE model.

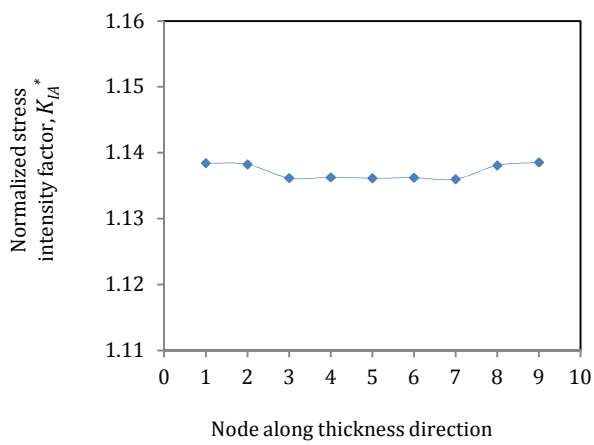


**Figure 6:** Normalized mode-I stress intensity factor distribution along thickness for 3-D FE model in Abaqus.

To ensure the accuracy of the proposed extended finite element model (X-FEM), normalized mode I SIFs versus different vertical crack distance are calculated for different values of second crack length and compared with the results of 2-D FE model (Abaqus software). Modeling stationary cracks using FEM needs the geometry of cracked body to be matched with the mesh. Therefore, for each case, a separate FEM model is constructed.

Figure 7 shows good correlation between the calculated SIFs at the crack tip using 2-D FEM and X-FEM. The difference between the X-FEM and Abaqus results in all cases is less than 2 percent.

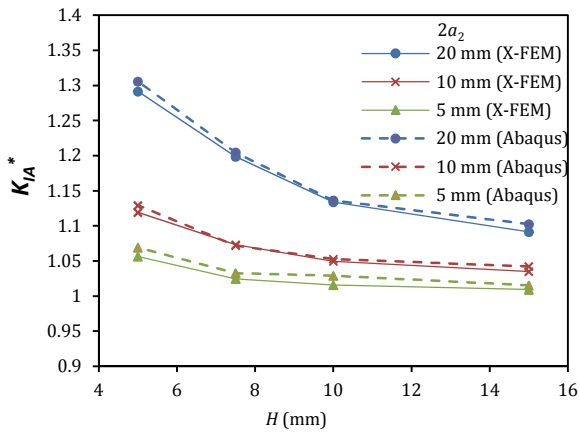


**Figure 7:** Validation of X-FEM model with Abaqus results.

### 4.3. Effect of the Crack Distance

Figs. 8-10 show the influence of the normalized vertical ($H^*$) and horizontal ($S^*$) distances on the interaction of stress intensity factor $K_{IA}^*$ at the inner tip of larger crack (point A). In the analyses, the normalized vertical ($H^*$) and horizontal ($S^*$) distances take the following values:

$$H^* = 1.5, 1.0, 0.9, 0.7, 0.5, 0.3$$
$$S^* = 1.5, 1.2, 1.0, 0.9, 08, 0.7, 0.6, 0.5, 0.4, 0.3, 0.2, 0.1, 0, -0.2$$

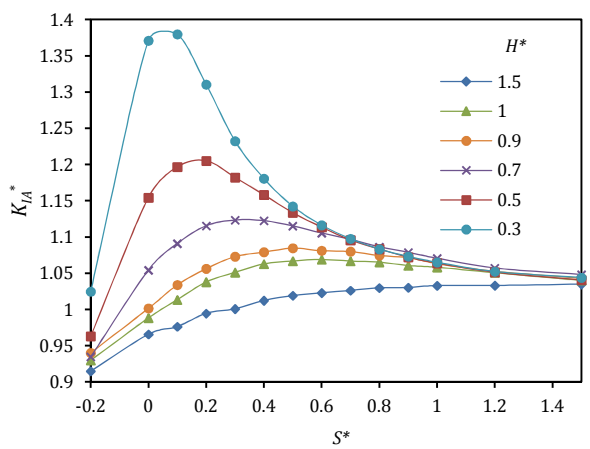


**Figure 8:** Normalized mode-I stress intensity factor distribution at inner tip of larger crack for similar offset cracks ($2a_1$=$2a_2$=20 mm).

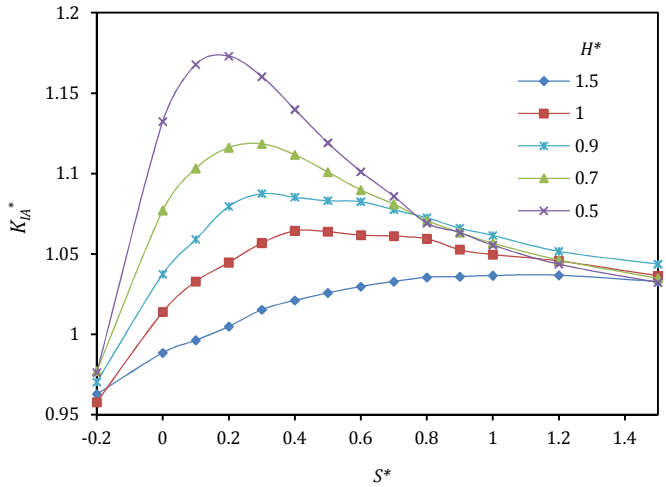


**Figure 9:** Normalized mode-I stress intensity factor distribution at inner tip of larger crack for dissimilar offset cracks ($2a_1$=20 mm, $2a_2$=10 mm).

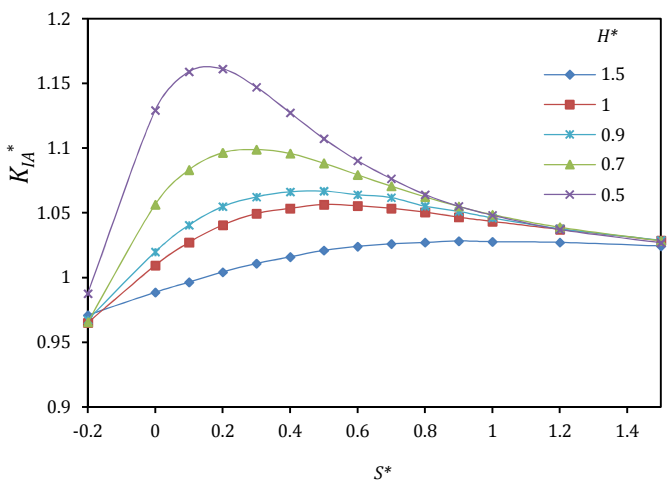


**Figure 10:** Normalized mode-I stress intensity factor distribution at inner tip of larger crack for dissimilar offset cracks ($2a_1$=20 mm, $2a_2$=5 mm).

The figures show that the mode-I stress intensity factor at the inner tip of larger crack increases as the nearest crack tips approach one another, but then declines as the tips pass. As is clear from these figures, the general shape of the curves and their values in the three figures, are approximately located in the same range. Another important point is that in high $H^*$, although the normalized in-plane crack separation ($S^*$) decreases, the stress intensity factor does not exceed a certain limit. For example, according to Fig. 8, in $H^*$=1.5, the stress intensity factor in comparison with an isolated crack, is maximally increased about 4%.

### 4.4. Effect of Smaller Crack Length

Figs. 11-13 show that normalized mode-I stress intensity factors are almost in the same range for different secondary crack length. This indicates that the normalized first mode stress intensity factor is an appropriate factor for describing the interaction effect. According to figure 12 in $H^*= 1.0$, the increase in the stress intensity factor in comparison with an isolated crack, is about 7%. Furthermore, maximum increase occurs when the lengths of two cracks are equal. According to figure 13, in $H^* = 0.9$, the maximum increase in the stress intensity factor for the length of second crack 2a2=20 mm is 8.5 % and for $2a_2$=10 mm is 8 %, and at the length of secondary crack $2a_2$=5 mm is equal to 6.5%. $K_{IA}^*$

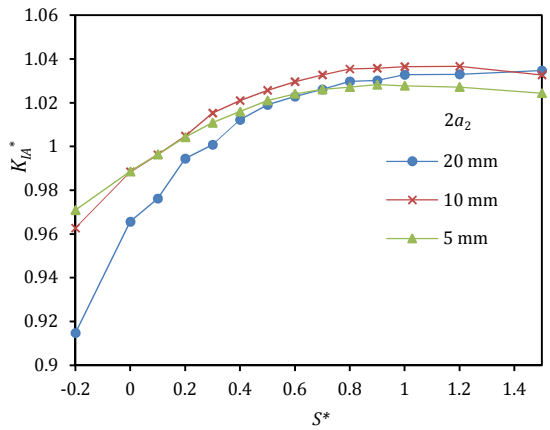


**Figure 11:** Comparison of normalized mode-I stress intensity factor at inner tip of larger crack for different secondary crack length ($H^*$=1.5).

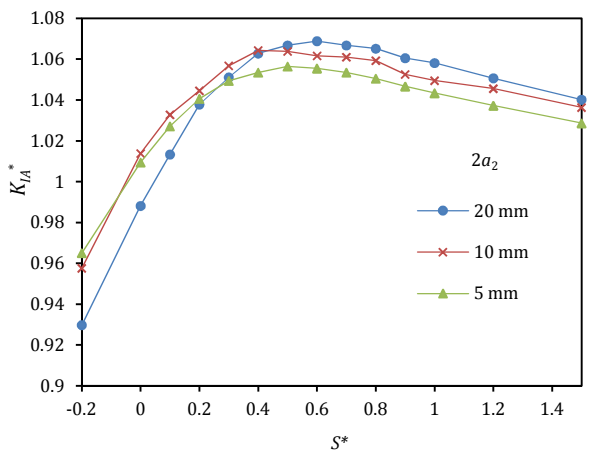


**Figure 12:** Comparison of normalized mode-I stress intensity factor at inner tip of larger crack for different secondary crack length ($H^*$=1.0).

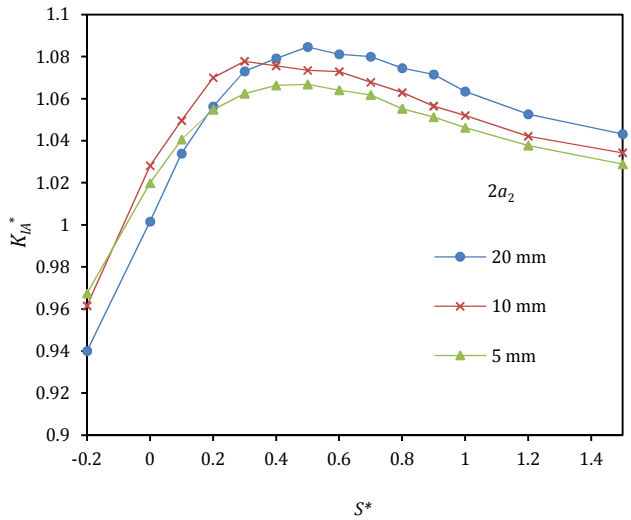


**Figure 13:** Comparison of normalized mode-I stress intensity factor at inner tip of larger crack factor for different secondary crack length ($H^*$=0.9).

The crack interaction and coalescence is most relevant to the mixed mode loading condition. The extent of $K_{II}/K_I$ ratio depends on the offset distance. Figs. 14 and 15 indicate that the mode-II stress intensity factor ($K_{II}$) is introduced when the nearest crack tips closely approach; the crack tips then actually experience a mixed mode-I and II condition during their interaction.

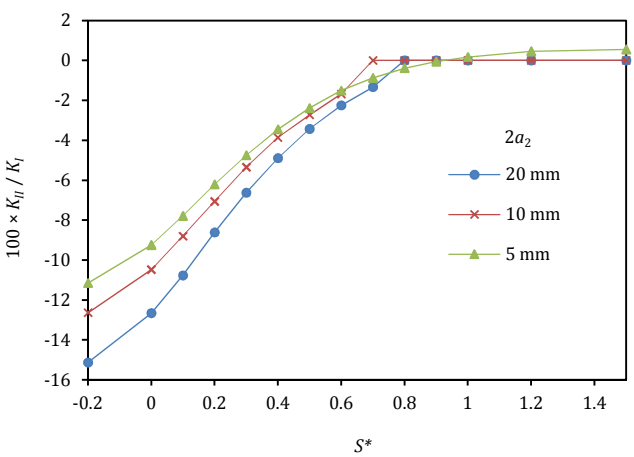


**Figure 14:** The ratio of mode-II to mode-I stress intensity factor at inner tip of larger crack factor for different secondary crack length ($H^*$=0.9).

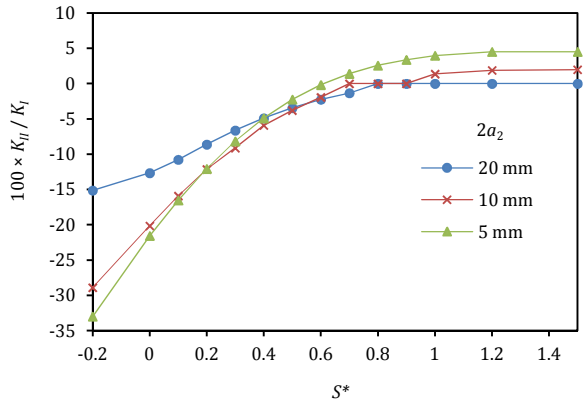


**Figure 15:** The ratio of mode-II to mode-I stress intensity factor at inner tip of smaller crack factor for different secondary crack length ($H^*$=0.9).

The mode-II stress intensity factor becomes significant and the sign changes from positive to negative as the crack tips approach and then pass. The absolute value of $K_{II}/K_I$ is larger for the inner tip of smaller crack.

The direction of crack growth under combined mode-I and II loading is only related to the $K_{II}/K_I$ ratio (Eq. (17)). The positive value of $K_{II}/K_I$ promotes a divergent path while its negative value a convergent one. The above results indicate that it is the mixed mode stressing condition experienced by the nearest tips of the offset cracks that leads to the change of crack growth direction and causes coalescence.

### 4.5. Crack Growth Simulation

In order to obtain detailed information about the interaction behavior of offset cracks, crack growth simulation is carried out for different configuration of cracks. In the analyses, the normalized vertical ($H^*$) and horizontal ($S^*$) distances take the following values:

$$H^* = 1.5, 1.0, 0.9, 0.7, 0.5, 0.3$$
$$S^* = 1.5, 1.2, 1.0, 0.9, 08, 0.7, 0.6, 0.5, 0.4, 0.3, 0.2, 0.1, 0, -0.2$$

In the simulation, plate specimen is subjected to displacement controlled loading and the crack path is determined according to procedure described in the previous section. In each configuration, the growth behavior is determined and it is specified whether propagating cracks run into the opponent crack or not. The crack paths obtained by the simulation for two configurations of cracks are shown in Figs. 16 and 17. Figure 16 shows the results for the specimen in which $H^*$=0.75, $S^*$=0.75 and $2a_2$=20 *mm*. In this case, the cracks grow to each other and coalescence of the crack tips would occur. Figure 17 shows the result for the specimen in which $H^*$=1.5, $S^*$=1.5 and $2a_2$=10 *mm*. In this case, the inner flaws did not grow significantly because the distance between the flaw tips is large. Finally, coalescence of the crack tips did not occur. Also, Table 4 presents the crack propagation paths of X-FEM simulation for some configurations.

| No. | Crack length ($mm$) | $S$ ($mm$) | $S^*$ | $H$ ($mm$) | $H^*$ | Fracture path coalescence |
|---|---|---|---|---|---|---|
| A-01 | | 30 | 1.5 | 30 | 1.5 | No |
| A-02 | $2a_1$=20 | 20 | 1 | 20 | 1 | Yes |
| A-03 | $2a_2$=20 | 15 | 0.75 | 15 | 0.75 | Yes |
| A-04 | | 10 | 0.5 | 10 | 0.5 | Yes |
| B-01 | | 20 | 2 | 20 | 2 | No |
| B-02 | $2a_1$=20 | 15 | 1.5 | 15 | 1.5 | No |
| B-03 | $2a_2$=10 | 10 | 1.0 | 10 | 1.0 | No |
| B-04 | | 7.5 | 0.75 | 7.5 | 0. 75 | Yes |
| C-01 | | 15 | 3.0 | 15 | 3.0 | No |
| C-02 | $2a_1$=20 | 10 | 2.0 | 10 | 2.0 | No |
| C-03 | $2a_2$=5 | 5 | 1.0 | 5 | 1.0 | No |

**Table 4:** Cracks paths results: X-FEM simulation.

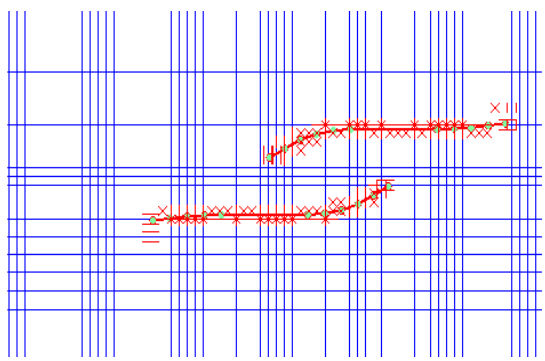

**Figure 16:** Simulated crack propagation paths for similar offset cracks ($H^*$=0.75, $S^*$=0.75, $2a_1$=20 $mm$, $2a_2$=20 $mm$).

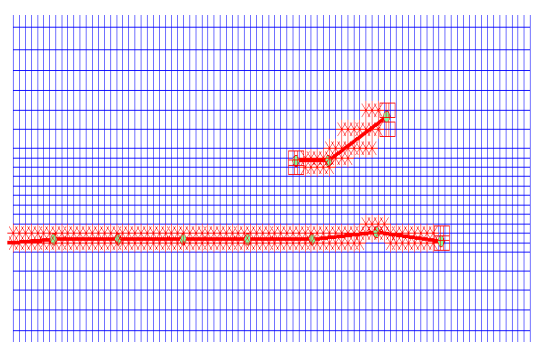

**Figure 17:** Simulated crack propagation paths for dissimilar offset cracks ($H^*$=1.5, $S^*$=1.5, $2a_1$=20 $mm$, $2a_2$=10 $mm$).

Simulation results of crack propagation paths for different configuration of offset cracks indicate that the coalescence of the crack tips will occur when the increase in the mode-I stress intensity factor in comparison with an isolated crack is about 7% or greater, and the ratio of the mode-II to mode-I stress intensity factor at the tip A is more than 1%.

According to Figures 8- 10 and 14, it could be concluded that for equal offset cracks ($2a_1=2a_2$), the following conditions are satisfied when $H^{*\leq} 1$ and $S^{*\leq} 1$. For dissimilar offset cracks ($2a_1\neq 2a_2$), these conditions are satisfied when $H^{*}< 1$ and $S^{*}< 1$. This could be a boundary for alignment and combination criteria for offset cracks.

### 4.6. Discussion of the Multiple Crack Treatment Rules

In order to assess the proximity rules in the FFS codes, the treatment of these codes is compared with the X-FE simulation results for some configurations in Table 5.

In the ASME and JSME codes, an absolute value is used for the alignment rule and the vertical distance $H$ is compared with a fixed separation distance of 12.5 mm. This implies that the interaction is not taken into account even though the interaction is important for large cracks. According to Table 5, the two cracks in A-02 and A-03 specimens are regarded as two non-aligned independent cracks (TNIC) in accordance with the ASME and JSME Codes; whereas the simulation results indicate that the cracks run in to each other. On the other hand, the two cracks in B-03, C-02 and C-03 specimens are regarded as aligned and combined cracks which this is not consistent with the simulation results. It can be asserted that the vertical distance $H$ should be a function of the size of cracks. However, in these codes, the combination rule is defined in terms of the larger crack. Compared to simulation results, this rule gives conservative evaluation.

In the API 579 the vertical distance $H$ is compared with the average of two crack lengths as the alignment rule. Also, in the BS 7910, FKM, R6 and A16 the direct distance $D$ is compared with the average of two crack lengths as the alignment rule. These codes, especially API 579, give overly conservative results compared to the simulation results, particularly, if the opponent crack is small. In the API 579, the two cracks of the specimens B02, B-03, C-02 and C-03 are treated to be aligned and combined as one single crack (OSC) as opposed to the simulation results, where the cracks did not run to each other. In these codes, the horizontal distance between two cracks $S$ is compared with the minimum crack length. It seems to be a reasonable criterion.

The alignment rule given by WES 2805 is a function of small crack length. Two cracks for specimens A-02, A-03 and B-04 are evaluated by WES 2805 to be non-aligned independent cracks which did not match with the simulation results. The proximity rule defined by this code seems to be non-conservative.

| No. | Crack length (mm) | $H$, $S$ (mm) | Fracture path coalescence (X-FEM results) | ASME & JSME | | | API 579 | | | BS7910, R6, A16 & FKM | | | WES-2805 | | | GB/T 19624 & FITNET | | | Proposed rules | | |
|---|---|---|---|---|---|---|---|---|---|---|---|---|---|---|---|---|---|---|---|---|---|
| | | | | Alignment | Combination | Resulted crack | Alignment | Combination | Resulted crack | Alignment | Combination | Resulted crack | Alignment | Combination | Resulted crack | Alignment | Combination | Resulted crack | Alignment | Combination | Resulted crack |
| A-01 | | 30 | N | N | | TNIC | N | | TNIC | N | | TNIC | N | | TNIC | N | | TNIC | N | | TNIC |
| A-02 | $2a_1$=20 | 20 | Y | N | | TNIC | Y | Y | OSC | N | | TNIC | N | | TNIC | Y | Y | OSC | Y | Y | OSC |
| A-03 | $2a_2$=20 | 15 | Y | N | | TNIC | Y | Y | OSC | N | | TNIC | N | | TNIC | Y | Y | OSC | Y | Y | OSC |
| A-04 | | 10 | Y | Y | | OSC | Y | Y | OSC | Y | Y | OSC | Y | Y | OSC | Y | Y | OSC | Y | Y | OSC |
| B-01 | | 20 | N | N | | TNIC | N | | TNIC | N | | TNIC | N | | TNIC | N | | TNIC | N | | TNIC |
| B-02 | $2a_1$=20 | 15 | N | N | | TNIC | Y | Y | OSC | N | | TNIC | N | | TNIC | N | | TNIC | N | | TNIC |
| B-03 | $2a_2$=10 | 10 | N | Y | Y | OSC | Y | Y | OSC | Y | Y | OSC | N | | TNIC | Y | Y | OSC | N | | TNIC |
| B-04 | | 7.5 | Y | Y | Y | OSC | Y | Y | OSC | Y | Y | OSC | N | | TNIC | Y | Y | OSC | Y | Y | OSC |
| C-01 | | 15 | N | N | | TNIC | N | | TNIC | N | | TNIC | N | | TNIC | N | | TNIC | N | | TNIC |
| C-02 | $2a_1$=20 | 10 | N | Y | Y | OSC | Y | Y | OSC | Y | N | TCC | N | | TNIC | N | | TNIC | N | | TNIC |
| C-03 | $2a_2$=5 | 5 | N | Y | Y | OSC | Y | Y | OSC | Y | Y | OSC | N | | TNIC | Y | Y | OSC | N | | TNIC |

Abbreviations: Y: Yes; N: No; OSC: One single crack; TCC: Two co-planar cracks;
TNIC: Two non-aligned independent cracks.

**Table 5:** Comparison of proximity rules among different codes.

In the GB/T 19624 and FITNET codes, the vertical distance between two cracks $H$ is compared with the minimum crack length as the alignment rule and the horizontal distance $S$ is compared with the minimum crack length as the combination rule. The evaluation of cracked geometries with these codes match with the simulation results in the most cases. The alignment rules defined by GB/T 19624 and FITNET give conservative evaluation only in some cases (B-03 and C-03). These codes seem to be reasonable criteria.

It is clear that, for two identical co-planar cracks, almost all the current FFS codes prescribe that a single enveloping crack with a length of $2a=4a+S$ should be adopted if the condition of $S/a< 2$ is satisfied. However, for two dissimilar co-planar cracks, the combination rule is different in various FFS codes. For example, for two interacting cracks with $a_1=2a_2$, the combination rule in BS7910, R6, A16, FKM, FITNET, GB/T19624 is $S/a_2< 2$, which is less than that of $S/a_2< 3$ in API579 and less than that of $S/a_2< 4$ in ASME code. The combination rules for co-planar cracks provided by ASME code and API579 give conservative evaluation.

As can be seen in Table 5, it seems that the proposed alignment and combination rules are in accordance with the X-FE simulation results and these rules could reduce the margin of conservativeness. This leads to more component life and less the costs of the component replacement.

## CONCLUSION

To investigate the effects of the interaction of cracks, extended finite element method has been utilized to simulate the brittle fracture of a plate containing two offset cracks. The effect of crack distances and lengths on the values of mode-I and mode-II stress intensity factors is evaluated. In addition, crack growth behavior is simulated based on linear elastic fracture mechanics approach. The mode-I stress intensity factor at the inner tip of two offset cracks increases by decreasing distance between the two cracks, and decreases by decreasing opponent crack length**.** The mode-II stress intensity factor is introduced when the nearest crack tips closely approach; the crack tips then actually experience a mixed mode-I and II condition during their interaction. The mode-II stress intensity factor becomes significant and the sign changes from positive to negative as the crack tips approach and then pass. Simulation results of crack propagation paths indicate that the coalescence of the crack tips will occur when the increase in the mode-I stress intensity factor in comparison with an isolated crack is about 7% or greater, and the ratio of the mode-II to mode-I stress intensity factor at the tip A is more than 1%. According to simulation results, the following conditions are satisfied when $H^{*\leq} 1$ and $S^{*\leq} 1$ for equal offset cracks ($2a_1=2a_2$), and when $H^{*}< 1$ and $S^{*}< 1$ for dissimilar offset cracks ($2a_1\neq 2a_2$). Therefore, the following alignment and combination rules are proposed for LEFM assessment:

$$\text{Alignment rule: } \begin{cases} H < \min(2a_1, 2a_2) & 2a_1 \neq 2a_2 \\ H \leq 2a_1 & 2a_1 = 2a_2 \end{cases}$$

$$\text{Combination rule: } \begin{cases} S < \min(2a_1, 2a_2) & 2a_1 \neq 2a_2 \\ S \leq 2a_1 & 2a_1 = 2a_2 \end{cases}$$

**Funding**

This research received no specific grant from any funding agency in the public, commercial or not-for-profit sectors.

**Conflict of interest**

None declared.

## References

AFCEN. (2005) RSE-M: Inservice Inspection Rules for the Mechanical Components of PWR Nuclear Islands. Paris: French Association for design, construction and in-service inspection rules for nuclear island components.

API. (2007) API 579-1/ASME FFS-1: Fitness-for-Service: American Petroleum Institute.

ASME. (2010). Boiler and Pressure Vessel Code Section XI Rules for Inservice Inspection of Nuclear Power Plant Components. New York: American Society of Mechanical Engineers.

British Energy Generation Ltd. (2006) R6: Assessment of the Integrity of Structures Containing Defects. Gloucester.

BS. (2005) BS 7910: Guide to Method for Assessing the Acceptability of Flaws in Metallic Structures. London: British Standards Institution.

Commissariat a L'Energie Atomique. (2002) A16: Guide for Defect Assessment and Leak Before Break Analysis. France.

CS. (2004) GB/T19624: Safety Assessment for In-Service Pressure Vessels Containing Defects. Beijing: Chinese Standards.

Erdogan, F., & Sih, G. (1963). On the crack extension in plates under plane loading and transverse shear. Journal of basic engineering, Vol. 85, pp. 519.

European Fitness for Service Network. (2008) FITNET Fitness-for-Service (FFS) – Procedure: Eds. M. Koçak, S. Webster, J.J. Janosch, R.A. Ainsworth, R. Koers.

FKM. (2004) Fracture Mechanics Proof of Strength for Engineering Components. Frankfurt am Main: Forschungskuratorium Maschinenbau (FKM).

Hasegawa, K., Saito, K., & Miyazaki, K. (2009). Alignment Rule for Non-Aligned Flaws for Fitness-for-Service Evaluations Based on LEFM. Journal of Pressure Vessel Technology, Vol. 131, No. 4, pp. 041403.

Jones, R., Atluri, S., Pitt, S., & Williams, J. (1995). Developments in the analysis of interacting cracks. Engineering Failure Analysis, Vol. 2, No. 4, pp. 307-320.

JSME. (2004) Codes for Nuclear Power Generation Facilities: Rules of Fitness for Service for Nuclear Power Plants: Japan Society of Mechanical Engineers.

Kamaya, M. (2008). Influence of the Interaction on Stress Intensity Factor of Semielliptical Surface Cracks. Journal of Pressure Vessel Technology, Vol. 130, No. 1, pp. 011406-011406.

Lam, K. Y., & Phua, S. P. (1991). Multiple crack interaction and its effect on stress intensity factor. Engineering Fracture Mechanics, Vol. 40, No. 3, pp. 585-592.

Miyazaki, K., Hasegawa, K., Saito, K., & Bezensek, B. (2009). Experimental Study of Ductile Fracture for Non-Aligned Multiple Flaws in a Plate. Paper presented at the ASME 2009 Pressure Vessels and Piping Conference, Prague, Czech Republic.

Moës, N., Dolbow, J., & Belytschko, T. (1999). A finite element method for crack growth without remeshing. International Journal for Numerical Methods in Engineering, Vol. 46, No. 1, pp. 131-150.

Murakami, Y., & Nemat-Nasser, S. (1982). Interacting dissimilar semi-elliptical surface flaws under tension and bending. Engineering Fracture Mechanics, Vol. 16, No. 3, pp. 373-386.

Sadowski, T., Marsavina, L., Peride, N., & Craciun, E.-M. (2009). Cracks propagation and interaction in an orthotropic elastic material: Analytical and numerical methods. Computational Materials Science, Vol. 46, No. 3, pp. 687-693.

Serier, B., Belhouari, M., & Bachir Bouiadjra, B. (2004). Numerical study of the interaction between an interfacial crack and a subinterfacial microcrack in bi-materials. Computational Materials Science, Vol. 29, No. 3, pp. 309-314.

Tan, J. T., & Chen, B. K. (2013). A new method for modelling the coalescence and growth of two coplanar short cracks of varying lengths in AA7050-T7451 aluminium alloy. International Journal of Fatigue, Vol. 49, No. 0, pp. 73-80.

Wes. (1997) Wes 2805: Methods of Assessment for Defects in Fusion welded Joints with Respect to Brittle Fracture and Failure due to Fatigue Crack Growth: The Japan Welding Engineering Society.

Yau, J. F., Wang, S. S., & Corten, H. T. (1980). A Mixed-Mode Crack Analysis of Isotropic Solids Using Conservation Laws of Elasticity. Journal of Applied Mechanics, Vol. 47, No. 2, pp. 335-341.

Yokobori, T., Uozumi, M., & Ichikawa, M. (1971). Interaction between non-coplanar parallel staggered elastic cracks(Interaction between two noncoplanar parallel staggered elastic cracks with narrow spacing, calculating stress intensity required for crack propagation). Tohoku University, Research Institute for Strength and Fracture of Materials, Reports, Vol. 7, pp. 25-47.